NASA/TM—2018-219950

# Analysis of the Influence of Layer Shifting on the Elastic Response and Damage Nucleation and Growth in Woven Composite Laminates

*Juan José Espadas-Escalante*
*The Ångström Laboratory, Uppsala University, Uppsala, Sweden*

*Brett A. Bednarcyk*
*Glenn Research Center, Cleveland, Ohio*

*Per Isaksson*
*The Ångström Laboratory, Uppsala University, Uppsala, Sweden*

September 2018

# NASA STI Program . . . in Profile

Since its founding, NASA has been dedicated to the advancement of aeronautics and space science. The NASA Scientific and Technical Information (STI) Program plays a key part in helping NASA maintain this important role.

The NASA STI Program operates under the auspices of the Agency Chief Information Officer. It collects, organizes, provides for archiving, and disseminates NASA's STI. The NASA STI Program provides access to the NASA Technical Report Server—Registered (NTRS Reg) and NASA Technical Report Server—Public (NTRS) thus providing one of the largest collections of aeronautical and space science STI in the world. Results are published in both non-NASA channels and by NASA in the NASA STI Report Series, which includes the following report types:

- TECHNICAL PUBLICATION. Reports of completed research or a major significant phase of research that present the results of NASA programs and include extensive data or theoretical analysis. Includes compilations of significant scientific and technical data and information deemed to be of continuing reference value. NASA counter-part of peer-reviewed formal professional papers, but has less stringent limitations on manuscript length and extent of graphic presentations.

- TECHNICAL MEMORANDUM. Scientific and technical findings that are preliminary or of specialized interest, e.g., "quick-release" reports, working papers, and bibliographies that contain minimal annotation. Does not contain extensive analysis.

- CONTRACTOR REPORT. Scientific and technical findings by NASA-sponsored contractors and grantees.

- CONFERENCE PUBLICATION. Collected papers from scientific and technical conferences, symposia, seminars, or other meetings sponsored or co-sponsored by NASA.

- SPECIAL PUBLICATION. Scientific, technical, or historical information from NASA programs, projects, and missions, often concerned with subjects having substantial public interest.

- TECHNICAL TRANSLATION. English-language translations of foreign scientific and technical material pertinent to NASA's mission.

For more information about the NASA STI program, see the following:

- Access the NASA STI program home page at http://www.sti.nasa.gov

- E-mail your question to help@sti.nasa.gov

- Fax your question to the NASA STI Information Desk at 757-864-6500

- Telephone the NASA STI Information Desk at 757-864-9658

- Write to:
  NASA STI Program
  Mail Stop 148
  NASA Langley Research Center
  Hampton, VA 23681-2199

NASA/TM—2018-219950

# Analysis of the Influence of Layer Shifting on the Elastic Response and Damage Nucleation and Growth in Woven Composite Laminates

*Juan José Espadas-Escalante*
*The Ångström Laboratory, Uppsala University, Uppsala, Sweden*

*Brett A. Bednarcyk*
*Glenn Research Center, Cleveland, Ohio*

*Per Isaksson*
*The Ångström Laboratory, Uppsala University, Uppsala, Sweden*

National Aeronautics and
Space Administration

Glenn Research Center
Cleveland, Ohio 44135

September 2018

## Acknowledgments

This work was partially supported by CONACYT (Mexico) under the scholarship 383215 provided to the first author.



*Level of Review*: This material has been technically reviewed by technical management.

Available from

NASA STI Program
Mail Stop 148
NASA Langley Research Center
Hampton, VA 23681-2199

National Technical Information Service
5285 Port Royal Road
Springfield, VA 22161
703-605-6000

This report is available in electronic form at http://www.sti.nasa.gov/ and http://ntrs.nasa.gov/

# Analysis of the Influence of Layer Shifting on the Elastic Response and Damage Nucleation and Growth in Woven Composite Laminates

Juan José Espadas-Escalante
The Ångström Laboratory
Uppsala University
SE-751 21 Uppsala, Sweden

Brett A. Bednarcyk
National Aeronautics and Space Administration
Glenn Research Center
Cleveland, Ohio 44135

Per Isaksson
The Ångström Laboratory
Uppsala University
SE-751 21 Uppsala, Sweden

## Abstract

The influence of relative layer shifting on the elastic and damage response of plain weave composite laminates is analyzed using a continuum damage mechanics approach in combination with the finite element method. First, the homogenized properties of the woven composite as a function of the number of layers and of layer shifting are presented. Next, the damage development in various shifting configurations is studied using different damage constitutive models for the matrix and the fiber bundles. It is shown that the impact of layer shifting on both the elastic response and the nonlinear damage response is significant. Most notably, the model captures changes in the damage mechanisms within the woven composite that occur due to layer shifting, resulting in stiffer, more brittle behavior, which has been shown experimentally in the literature. Model results in the linear and nonlinear regimes are shown to be consistent with both an independent analytical model and reported experiments.

## 1.0 Introduction

An advantage of woven composites with respect to the traditionally used unidirectional tape laminates is their lower production costs. However, their use has been restricted partially due to a lack of understanding of their structural integrity and damage evolution (Ref. 1). Woven composites are typically analyzed numerically using discretized repeating unit cells (RUCs) in finite element models. Continuum damage mechanics can be included in these models to capture the nucleation and coalescence of micro cracks in the matrix and fiber bundles (yarns) (Refs. 2 and 3). One common approach to model elastic and damage development is to assume that a repeating unit cell of a single layer represents the whole laminate, i.e., geometric variabilities between layers in the composite are disregarded. The parameters used in continuum damage models are often obtained by fitting to experiments (Ref. 4), from sub-scale damage simulations (Refs. 5 and 6) or from qualitative observations (Ref. 7). The underlying failure mechanisms in the woven composites constituents are often assumed different. For example, Barbero et al. (Ref. 4)

modeled a woven laminate using a repeating unit cell of one layer. These authors considered damage in the fiber bundles by calibrating parameters from experiments and considered the matrix to be elastic and free of damage. Uniaxial tensile tests of woven composite laminates were reported to be in agreement with their results. Other works have considered failure in the fiber bundles and matrix simultaneously (Refs. 7 to 9). Blackketter et al. (Ref. 7) used damage parameters based on observations in shear failure and considered a remaining stiffness due to friction. Zako et al. (Ref. 8) considered an isotropic damage model for the matrix and an anisotropic damage model in the fiber bundles. Their anisotropic damage model was based on the orthotropic Hoffman's failure criteria (Ref. 10). Matveev et al. (Ref. 9) went one step further by considering fiber strength variabilities in the fiber bundles and a progressive degradation of the matrix stiffness. They considered a repeating unit cell based on a single woven layer and obtained a global stress-strain curve which was similar to the laminate with perfectly aligned layers tested by Ito and Chou (Ref. 11). More recently, Fagiano et al. (Ref. 12) performed an analysis using repeating unit cells with several layers built from micrographs including many mesostructural imperfections (Ref. 12) leading to quite computationally expensive models. Green et al. (Ref. 13) showed that using repeating unit cells built from micrographs, led to better results since more realistic imperfections are considered. On the other hand, very simplified analytical models, such as the one proposed by Gao et al. (Ref. 14), have reported consistency with experiments. Their model disregarded yarns' undulation, which can have a significant effect on the damage evolution (Refs. 12 and 15).

The most important mesostructural variabilities that must be considered in order to use simpler, but still accurate, RUCs is a current research topic (Refs. 16 and 17). Layer shifting is a miscrostructural imperfection typically ignored e.g. (Refs. 4, 8, 9, 18 to 20), even though it has been reported to affect the overall response of woven composites (Refs. 11, 21 to 23) significantly. Previous works have shown that strain fields (Ref. 24) and stress fields (Ref. 25) as well as the global mechanical response, are affected (Refs. 11 and 26).

This study explores the impact of layer shifting on the global initial elastic response of woven composites and on the consequent damage nucleation and growth in the woven composites constituents. Two distinct damage models have been employed. The first represents matrix damage and has been applied to model the response of the pure matrix regions in the composite, along with the transverse and shear responses of the fiber bundles. For the longitudinal response of the fiber bundles, a second damage model, which accounts for the fiber Weibull statistics, has been employed.

## 2.0 Continuum Damage Models

Two separate continuum damage models have been employed herein. The first is applied to the pure matrix regions in the composite as well as the transverse and shear behavior of the fiber bundles.

### 2.1 Matrix and Transverse/Shear Fiber Bundle Directions

The continuum damage model for the polymer matrix and transverse/shear fiber directions assumes that the elastic strain energies in the damaged and undamaged materials follow a similar form. For small deformations and adiabatic processes, the Gibbs free energy density is given by (Refs. 5, 27, and 28),

$$\chi = (2\rho)^{-1}\boldsymbol{\sigma}:\boldsymbol{\varepsilon} = (2\rho)^{-1}\boldsymbol{\sigma}:\mathbf{D}:\tilde{\mathbf{C}}^{-1}:\mathbf{D}:\boldsymbol{\sigma} \tag{1}$$

where $\rho$ is the density, $\boldsymbol{\sigma}$ is the Cauchy stress tensor, $\boldsymbol{\varepsilon}$ is the infinitesimal strain tensor, $\tilde{\mathbf{C}}$ is the stiffness matrix and the damage tensor $\mathbf{D} = (1 - D_{ij})^{-1}$ contains the damage parameters $D_{ij}$, with $i, j = 1, 2, 3$. The

index 1 refers to the fiber direction and 2-3 to the transverse planes. The values of $D_{ij}$ range from 0 (undamaged material) to 1 (completely damaged material). In unabridged notation, $\chi$ can be written as,

$$\chi = \frac{1}{2\rho}\left[\frac{\sigma_{11}^2}{(1-D_{11})^2\tilde{E}_{11}} + \frac{\sigma_{22}^2}{(1-D_{22})^2\tilde{E}_{22}} + \frac{\sigma_{33}^2}{(1-D_{33})^2\tilde{E}_{33}} - \left(\frac{\tilde{\nu}_{21}}{\tilde{E}_{22}} + \frac{\tilde{\nu}_{12}}{\tilde{E}_{11}}\right)\frac{\sigma_{11}\sigma_{22}}{(1-D_{11})(1-D_{22})} - \left(\frac{\tilde{\nu}_{32}}{\tilde{E}_{33}} + \frac{\tilde{\nu}_{23}}{\tilde{E}_{22}}\right)\frac{\sigma_{22}\sigma_{33}}{(1-D_{22})(1-D_{33})} - \left(\frac{\tilde{\nu}_{31}}{\tilde{E}_{33}} + \frac{\tilde{\nu}_{13}}{\tilde{E}_{11}}\right)\frac{\sigma_{11}\sigma_{33}}{(1-D_{11})(1-D_{33})} + \frac{\sigma_{12}^2}{2(1-D_{12})^2\tilde{G}_{12}} + \frac{\sigma_{23}^2}{2(1-D_{23})^2\tilde{G}_{23}} + \frac{\sigma_{13}^2}{2(1-D_{13})^2\tilde{G}_{13}}\right] \tag{2}$$

where $\tilde{\nu}_{ij}$ are the Poisson's ratios, $\tilde{E}_{ij}$ and $\tilde{G}_{ij}$ are the normal and the shear elastic moduli and the tilde refers to the undamaged property. Now, let **C** denote the damaged stiffness tensor, i.e., $\mathbf{C}^{-1} = \mathbf{D} : \tilde{\mathbf{C}}^{-1} : \mathbf{D}$. Then, one obtain from Equation (2),

$$\mathbf{C}^{-1} = \rho\frac{\partial^2\chi}{\partial\boldsymbol{\sigma}^2} \tag{3}$$

Moreover, it is assumed that damage is developed when a damage surface of the form (Refs. 5 and 6),

$$f = \underbrace{\sqrt{\mathbf{Y}:\mathbf{H}:\mathbf{Y}}}_{\hat{g}} - \left(\underbrace{c_1\left(e^{\frac{\delta}{c_2}} - 1\right)}_{\gamma} + \gamma_0\right) \geq 0 \tag{4}$$

controls the damage evolution. In Equation (4) **H** is defined as a tensor in Voigt notation with components that are characteristic of the material (to be defined later). These components relate the interaction among the different damage variables $D_{ij}$ through the damage driving force **Y**. Thus, $\mathbf{Y} : \mathbf{H} : \mathbf{Y}$ ($\hat{g}$) gives a scalar value closely related to the Griffith energy. The damage driving force **Y** is energy conjugate to **D**,

$$\mathbf{Y} = \rho\frac{\partial\chi}{\partial\mathbf{D}} \tag{5}$$

The second term in Equation (4), $\gamma$, corresponds to a hardening-softening function depending on the material parameters $c_1$, $c_2$, the onset of damage growth $\gamma_0$, and a hardening variable $\delta$. The damage growth is given by,

$$\dot{\mathbf{D}} = \dot{\lambda}\frac{\partial f}{\partial\mathbf{Y}} \tag{6}$$

where $\dot{\lambda}$ is a so-called damage multiplier and that represents the magnitude of the damage increment and $\partial f/\partial\mathbf{Y}$ its direction. It is here assumed that hardening rate $\dot{\delta}$ is related to $\dot{\lambda}$ (Ref. 5) as,

$$\dot{\delta} = \dot{\lambda}\frac{\partial f}{\partial\gamma} \tag{7}$$

Karush-Kuhn-Tucker-type loading-unloading conditions are applied to restrict the admissible values of $\dot{\lambda}$ and $\dot{f}$,

$$\dot{\lambda} \geq 0; \quad f \leq 0; \quad \dot{\lambda} f = 0 \tag{8}$$

The first condition ensures irreversibility of the damage process, the second condition is related to the damage surface and the third condition is a balance law for the damage evolution. Therefore, the value of $\dot{\lambda}$ is determined provided that damage is evolving ( $f = \dot{f} = 0$ ), i.e.,

$$\dot{f} = \frac{\partial f}{\partial \mathbf{Y}} : \dot{\mathbf{Y}} + \frac{\partial f}{\partial \gamma} \dot{\gamma} = 0, \; f = 0 \tag{9}$$

One observes that Equations (6) to (9) are inspired from classical theories of associated plasticity.

Since $\mathbf{Y} = \mathbf{Y}(\varepsilon, \mathbf{D})$ and $\gamma = \gamma(\delta)$, their corresponding rates can be obtained. Thus, using the rates together with Equations (6) and (7), and by considering in Equation (4) that $\partial f/\partial \gamma = -1$, one can express $\dot{\lambda}$ using Equation (9), i.e.,

$$\dot{\lambda} = -\frac{\frac{\partial f}{\partial \mathbf{Y}} : \frac{\partial \mathbf{Y}}{\varepsilon}}{\frac{\partial f}{\partial \mathbf{Y}} : \frac{\partial \mathbf{Y}}{\partial \mathbf{D}} : \frac{\partial f}{\partial \mathbf{Y}} + \frac{\partial \gamma}{\partial \delta}} : \dot{\varepsilon} \tag{10}$$

Therefore, together with Equation (7), the hardening evolution is,

$$\dot{\delta} = -\dot{\lambda} \tag{11}$$

The numerical implementation of this damage model is shown in the pseudocode given in Figure 1.

| | |
|---|---|
| $\boldsymbol{\varepsilon}^n = \boldsymbol{\varepsilon}^{n-1} + (\Delta\boldsymbol{\varepsilon})^n$ | Calculate the current strain at the step $n$ |
| $\dot{\boldsymbol{D}}^n = \dot{\boldsymbol{D}}^{n-1}; \dot{\delta}^n = \dot{\delta}^{n-1}$ | Retrieve the damage variables from $n-1$ |
| $k = 0$ | Initialize dummy variable for iteration |
| **DO** | |
| $\boldsymbol{C}_k^n; \boldsymbol{\sigma}_k^n = \boldsymbol{C}_k^n : \boldsymbol{\varepsilon}_k^n; \boldsymbol{Y}_k^n; \gamma_k^n$ | Update at iteration $k$ |
| $g = \hat{g} - \hat{\gamma}$ | Compute the damage threshold |
| **IF** $g < 0$ | Evaluate if there is damage |
| **EXIT** | Exit `DO` if there is not damage |
| **ELSE** | |
| $k = k + 1$ | Continue iterating |
| $\dot{\lambda}$ | Compute the damage multiplier |
| $\dot{\boldsymbol{D}}_k^n = \dot{\boldsymbol{D}}_{k-1}^n + \dot{\lambda}\left(\frac{\partial f}{\partial \boldsymbol{Y}}\right)_{k-1}$ | Compute the damage variables at $k$ |
| $\delta_k^n = \delta_{k-1}^n - \dot{\lambda}$ | |
| **ENDIF** | |
| **ENDDO** | |
| $\dot{\boldsymbol{D}}^n = \dot{\boldsymbol{D}}_k^n; \dot{\delta}^n = \dot{\delta}_k^n$ | Update the damage variables |

Figure 1.—Pseudocode for the numerical implementation of the damage model.

### 2.2 Fiber Direction

The damage developed in the fiber direction of a unidirectional fiber bundle, $D_{11}^{FIB}$, is based on a cumulative probability of the fibers failure, $F(\hat{\sigma})$, at a stress $\hat{\sigma}$ following a statistical Weibull distribution (Refs. 28 and 29),

$$D_{11}^{FIB} = F(\hat{\sigma}) = 1 - e^{-\alpha\hat{\sigma}^{\beta}} \tag{12}$$

where $\alpha$ and $\beta$ are parameters related to the average strength of the fiber bundle and its distribution, respectively. These are in turn related to the critical stress to failure of the fiber bundle, $\sigma_b^{cr}$ (Ref. 28),

$$\sigma_b^{cr} = (\alpha\beta e)^{-1/\beta} \tag{13}$$

The parameters used to describe the damage evolution of the fiber bundle in the fiber direction, will be given in the next section.

## 3.0 Material Properties

### 3.1 Polymer Matrix

Typical properties of an epoxy are used for the matrix and are given in Table I. The constants $c_1$, $c_2$ and $\gamma_0$ and the components in of the matrix **H** used in Equation (4) estimated from experiments in previous work (Refs. 5 and 6),

$$\mathbf{H}^{\text{polymer}} := \begin{bmatrix} 0.75 & 0 & 0 & 0 & 0 & 0 \\ 0 & 0.75 & 0 & 0 & 0 & 0 \\ 0 & 0 & 0.75 & 0 & 0 & 0 \\ 0 & 0 & 0 & 0.55 & 0 & 0 \\ 0 & 0 & 0 & 0 & 0.55 & 0 \\ 0 & 0 & 0 & 0 & 0 & 0.55 \end{bmatrix} \tag{14}$$

Note that this matrix describes an isotropic damage evolution in Equation (4), since the normal components $H_{11} = H_{22} = H_{33}$ and the shear components $H_{44} = H_{55} = H_{66}$. The stress-strain curve for this material model is shown in Figure 2(a).

TABLE I.—MATERIAL CONSTANTS FOR THE ISOTROPIC EPOXY POLYMER MATRIX (REF. 6)

| $\tilde{E}$ | $\tilde{\nu}$ | $c_1$ | $c_2$ | $\gamma_0$ |
|---|---|---|---|---|
| 3 GPa | 0.38 | 25.7 MPa | –2.8 | 0.45 MPa |

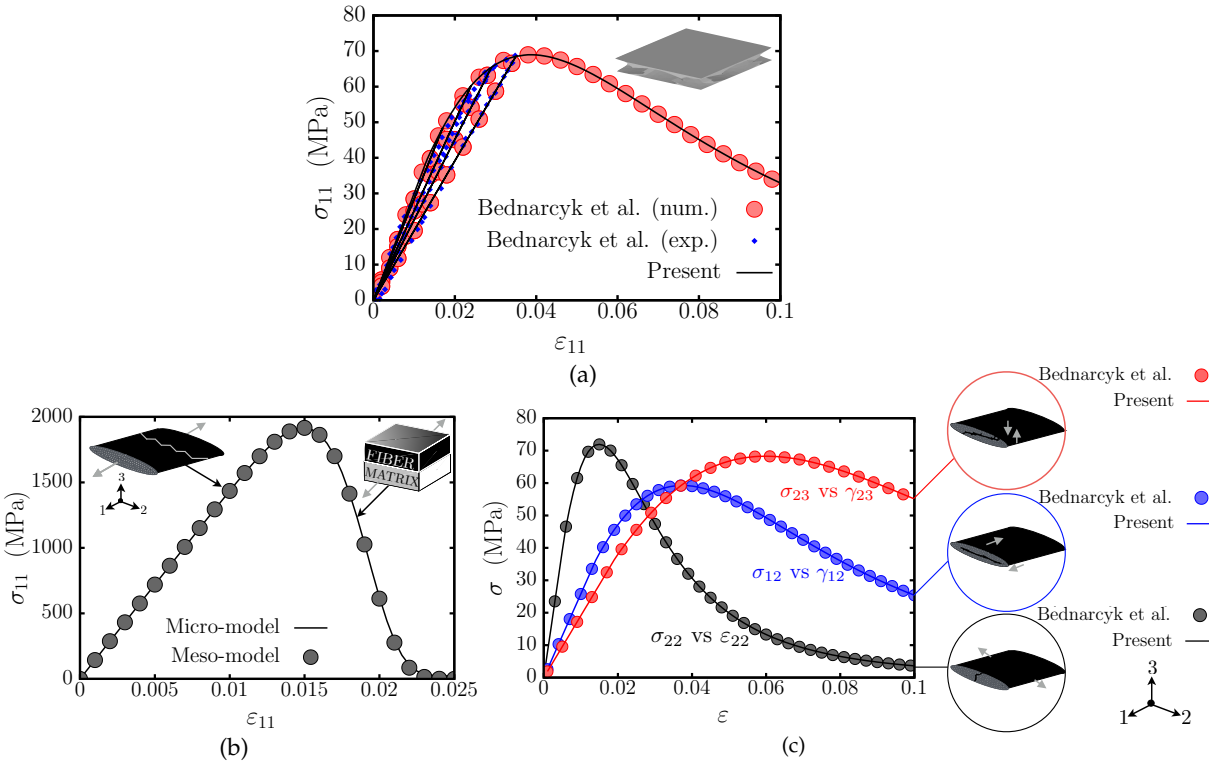


Figure 2.—Stress-strain curves for the damage material models implemented. (a) Matrix, (b) fiber bundle in the fiber direction, (c) fiber bundle in the transverse/shear directions. Experimental (exp.) and numerical (num.) comparison with Bednarcyk et al. (Ref. 5).

## 3.2 Fiber Bundle Properties

The homogenized elastic properties of the fiber bundles for a $V_f$ of 0.49, are presented in Table II.

To describe the damage evolution in the fiber direction of the fiber bundle used herein, a finite element model consisting of a T-300 Toray (Ref. 30) dry carbon fiber bundle and an epoxy matrix were used in an isostrain (Voigt) configuration, referred to here as the micro-model, where damage evolution was considered in both the dry fiber bundles and the matrix. The elastic and damage constitutive behavior of such a dry carbon fiber bundle is well known (Refs. 28 and 30) and it has been previously used for strength prediction (Ref. 28). The T-300 Toray dry carbon fiber bundle has a $\sigma_b^{cr}$ = 3 GPa and its damage evolution is described with a Weibull parameter $\beta$ = 8.9 (Refs. 28 and 30) in Equations (12) and (13). The damage constitutive behavior for the matrix previously described is used. This micro-model was subjected to uniaxial extension, Figure 2(b), and a new critical stress, $\sigma_b^{cr}$ = 1917 MPa, was found, Figure 2(b). Assuming a Weibull parameter identical to that of a dry fiber bundle $\beta$ = 8.9, the damage evolution in the fiber direction is described for the fiber bundle using Equations (12) and (13) and referred to as the meso-model in Figure 2(b). Note also that in these stress-strain curves, a more abrupt degradation is obtained, in comparison to the damage development in other directions, Figure 2(c).

To describe the damage evolution in the transverse/shear fiber bundle directions, the damage constants $c_1$, $c_2$ and $\gamma_0$ (Table II) and the components of the matrix **H** used in Equation (4) were obtained from micromechanics simulations using the generalized method of cells model (Ref. 31) and reported in previous works (Refs. 6 and 32). This method is useful for finding homogenized nonlinear constitutive relations for multiphase materials, particularly if experimental data are unavailable. Moreover, it has been

TABLE II.—MATERIAL CONSTANTS FOR THE HOMOGENIZED CARBON FIBER BUNDLES FOR A GIVEN $V_f$ (REF. 6)

| $\tilde{E}_{11}$ | $\tilde{E}_{22} = \tilde{E}_{33}$ | $\tilde{\nu}_{12} = \tilde{\nu}_{13}$ | $\tilde{\nu}_{23}$ | $\tilde{G}_{12} = \tilde{G}_{13}$ | $\tilde{G}_{23}$ | $c_1$ | $c_2$ | $\gamma_0$ | $m$ | $\sigma_b^{cr}$ |
|---|---|---|---|---|---|---|---|---|---|---|
| 144 GPa | 7.84 GPa | 0.29 | 0.39 | 1.91 GPa | 2.58 GPa | 63 MPa | –4 | 0.45 MPa | 8.9 | 1917 MPa |

chosen since it is purely based in a multiscale approach and experimental calibration is avoided, cf. (Refs. 6, 31, and 33) for further details. The matrix **H** for the fiber bundles is also taken from (Refs. 6 and 32) as,

$$\mathbf{H}^{\text{fiber bundle}} := \begin{bmatrix} 0 & 0 & 0 & 0 & 0 & 0 \\ 0 & 3.10 & 0.77 & 0 & 0 & 0 \\ 0 & 0.77 & 3.10 & 0 & 0 & 0 \\ 0 & 0 & 0 & 3.00 & 0 & 0 \\ 0 & 0 & 0 & 0 & 1.60 & 0 \\ 0 & 0 & 0 & 0 & 0 & 3.00 \end{bmatrix} \tag{15}$$

where the terms $H_{44}$, $H_{55}$ and $H_{66}$ correspond to the 1-2, 2-3 and 1-3-directions, respectively. The absence of the $H_{11}$ component means that no damage is developed in the fiber direction, which is instead accounted for by the model discussed in the Section 2.2. The terms $H_{23} = H_{32}$ are related to coupled damage in the 2 and 3-directions. Observe that in this case, the damage evolution is described in Equation (4) is not isotropic, as it was for the matrix. The stress-strain curves of the matrix and fiber bundles in the transverse/shear directions are presented in Figure 2(c).

The stress-strain curves shown in Figure 2, have been verified via comparison to the results in (Refs. 5 and 32).

## 4.0 Woven Composite Models

A two-layered laminate, with each layer containing a plain weave composite, model is shown in Figure 3(a). Each layer has a wavelength $\lambda = 0.4$ mm, yarn width $W_y = 0.18$ mm and a waviness ratio of $WR = t_l/\lambda = 1/4$, with $t_l$ being the layer thickness. The shifting, $\phi$, is defined as the relative position of the upper layer with respect to the lower one in the $y$-direction, ranging from $\phi = 0$ (no shifting) to $\phi = 0.5\lambda$ (maximum shifting) with every geometry keeping a constant volume fraction. To study the effect of the number of layers, four-layered laminates with the no shifting and maximum shifting configurations were also analyzed. Using TexGen (Ref. 34), each layer was discretized with a conformal mesh using standard quadratic tetrahedral elements with about $300 \cdot 10^3$ degrees of freedom in each layer. The mesh choice was based on a mesh refinement analysis by comparing the $V_f$ and the linear-elastic homogenized Euclidean norm of the stiffness matrix ($\left\|\tilde{\mathbf{C}}\right\|_2$), Figure 3(b). Observe that the $V_f$ slightly changes as the mesh is being refined because the mesh is not based on a fixed geometry but generated with TexGen (Ref. 34). This feature in TexGen has been observed previously, see e.g., (Ref. 35). It should also be noted that energy regularization has not been implemented herein. Therefore, localization and softening of the material models could lead to a mesh dependency (Refs. 5 and 36). However, the trends and conclusions made with these analyses are not expected to change drastically with further mesh refinements, since similar results were achieved with a coarser mesh (about $50 \cdot 10^3$ degrees of freedom).

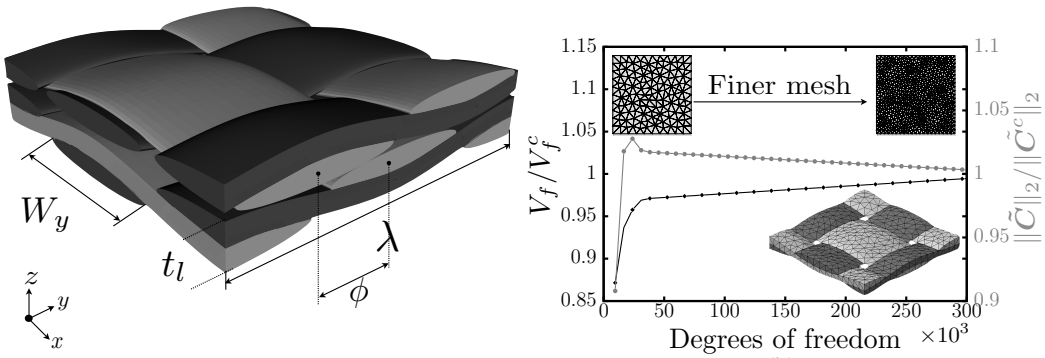


(a) (b)

Figure 3.—Models. (a) Geometry, (b) normalized volume fraction $V_f$ and norm of the stiffness matrix $\left\|\tilde{\mathbf{C}}\right\|_2$ with their convergent values ($^c$) in each layer as function of the degrees of freedom with the mesh shown. Matrix has been removed for visualization.

### 4.1 Boundary Conditions

In order to represent a woven laminate with a finite number of layers, periodic boundary conditions (BCs) are defined only in the *x*-*y*-plane (Figure 3(a)),

$$u_m^+ - u_m^- = \overline{\varepsilon}_{mn}\left(x_n^+ - x_n^-\right) \tag{16}$$

where $u_m$ are displacements, $\overline{\varepsilon}_{mn}$ the infinitesimal Cauchy strain tensor, $x_n$ the nodal positions, + and – opposite boundaries, $m, n=x, y$ and Einstein's summation convention prevails. For the *z*-direction load cases, Dirichlet BCs were imposed, i.e.,

$$u_m = \overline{\varepsilon}_{mn} x_n \tag{17}$$

while keeping the in-plane periodicity. Another mix of Neumann-periodic BCs was also explored, but a better convergence was reached with Dirichlet BCs for the nonlinear simulations. It is worth mentioning that, although Dirichlet BCs give higher stiffness than Neumann BCs in a single repeating unit cell (Refs. 37 and 38), the initial out-of-plane properties with both BCs were similar, since these out-of-plane properties do not depend strongly on the type of BCs imposed c.f. (Refs. 39 and 40). An additional case of periodic BCs in the in-plane and out-of-plane directions was considered in a repeating unit cell consisting of one single lamina. This represents a thick laminate where all the layers are perfectly aligned on top of each other and will be used for comparison purposes in the elastic response.

## 5.0 Results and Discussion

### 5.1 Influence of the Number of Layers on the Global Elastic Behavior

The woven laminate effective elastic properties are denoted as $E_{kl}$, $\nu_{kl}$, $G_{kl}$ with $k, l = x, y,$ z referring to the global Cartesian coordinate system in Figure 3(a). Recall that the layers are shifted only in the *y*-direction. The variation of the global in-plane modulus of elasticity $E_{xx}$ and in-plane Poisson's ratio $\nu_{xy}$ with the number of layers is shown in Figure 4 for the no shifting and maximum shifting models. These two properties, which were found to be the most sensitive to the number of layers, are normalized with the value obtained with one layer using periodic boundary conditions in all *x*-*y*-*z* directions simultaneously, referred to herein as PBCs, simulating a laminate with many aligned layers.

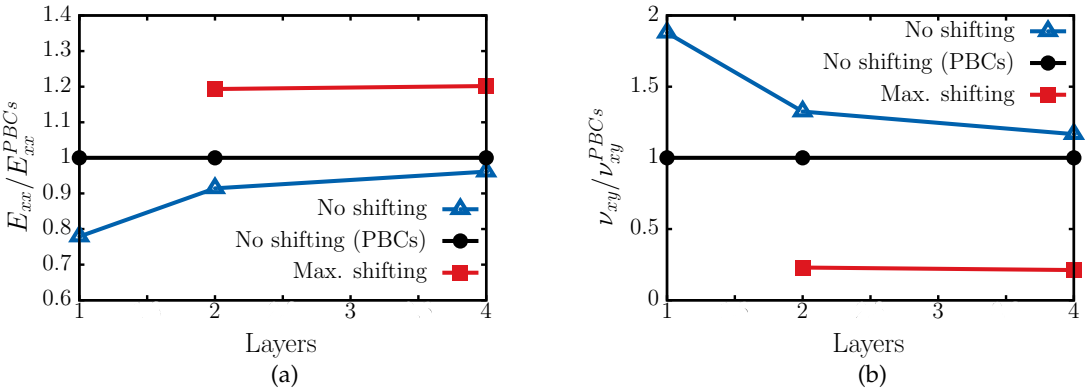


Figure 4.—Variation of the laminate properties with the number of layers normalized with the values achieved with PBCs simulating a laminate with several layers. (a) $E_{xx}$, (b) $\nu_{xy}$.

From Figure 4, it can be seen that when the layers are perfectly aligned on top of each other (no shifting), there is a significant difference from one to two layers, while the results for four layers appear to be approaching the PBC results asymptotically, Figure 4(a) and (b). This behavior is expected base on homogenization theory, wherein a convergent value is found when the number of repeating unit cells increase (Refs. 37 and 39).

When the woven laminate is in a maximum shifting configuration, the values in $E_{xx}$ and $\nu_{xy}$ from two to four layers remain constant, Figure 4. This suggests that only two laminates in a maximum shifting configuration, have a significant impact in woven laminates with more layers. This stiffening is related to the in-plane extension and out-of-plane shear coupling, as it will be detailed later. The value of $E_{xx}$ in this maximum shifting configuration can be 20% higher in $E_{xx}$, Figure 4(a), and $\nu_{xy}$ can be several times lower, Figure 4(b), with respect to the value predicted for a laminate with perfectly aligned layers. In the next section, it is shown that this magnitude of layer shifting impact on $E_{xx}$ is consistent with experimental observations and an independent analytical model.

In the results of both the perfectly aligned and maximum shifting models shown in Figure 4, it can be seen that two layers represent fairly well the elastic properties of a laminate of several layers. Clearly, a two layer model provides much more accuracy than a single layer model while remaining significantly more computational efficient than a four (or more) layer model. As such, the remaining results presented focus on two layer models.

## 5.2 Influence of Layer Shifting on the Global Elastic Behavior

While the previous section considered only the minimum and maximum shifting cases, in this section, the variation of the homogenized elastic properties as a function of the layer shifting is addressed. These properties have been normalized by their initial values without shifting (superscript 0). Since the layer shifting ($\phi$) goes from zero when the layers are perfectly aligned to half of the wavelength, $0.5\lambda$, when the layers are completely shifted, the value of $\phi$ has been normalized with the wavelength, $\lambda$.

Plots of the variation of the elastic properties as a function of the layer shifting are presented in Figure 5(a) and (b). In Figure 5(a), additional results from an analytical model due to Ito and Chou (Ref. 11) are shown for comparison. Details of this analytical model are given in the Appendix. Most of the properties vary nonlinearly with the layer shifting, with the greatest departure from the zero shifting case occurring at the maximum shifting. Observe that the trends in most of the properties follow a similar trend in both the numerical and analytical results. The most significant difference is in the $E_{zz}$ property, which seems to be influenced by the undulations of the neighboring fiber bundles considered in the finite element model.

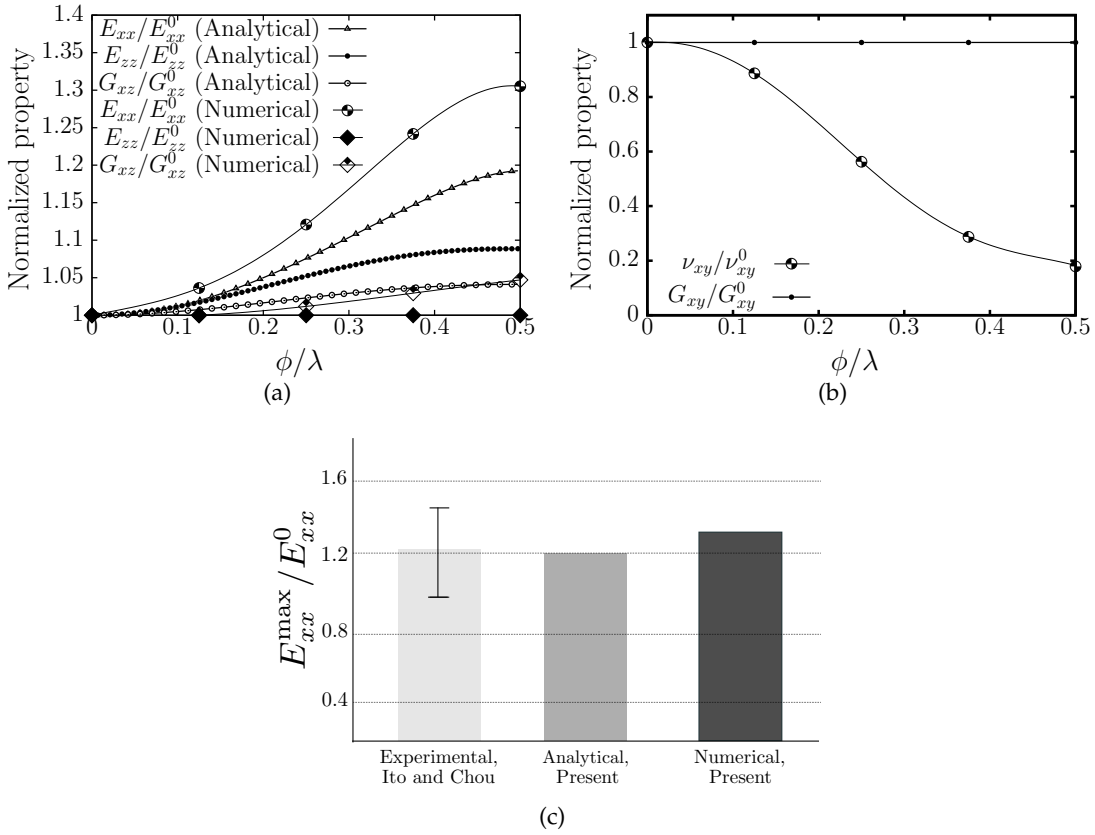


Figure 5.—Properties at different shifting configurations ($\phi/\lambda$) normalized with the initial value in the no shifting configuration ($^0$). (a) In-plane and out-of-plane modulus of elasticity and shear modulus for the analytical and numerical models, (b) in-plane shear modulus and Poisson's ratio (only numerical), (c) comparison for the maximum variation of $E_{xx}$ with experimental data of Ito and Chou (Ref. 11).

In Figure 5, it is shown that the most drastic effect of layer shifting is on $E_{xx}$ (increase of up to 30%) and $\nu_{xy}$ (decrease of up to 80%). The reason for the increase in global $E_{xx}$ and the reduction in $\nu_{xy}$ as function of $\phi/\lambda$ can be illustrated by using the simplified two-dimensional model (Ref. 11) detailed in the Appendix. In this simplified approach, the laminate elastic properties, obtained using classical laminate theory, are dependent on the **A** matrix. In classical laminate theory, it is well known that the $A_{16}$ and $A_{26}$ components of **A** are related to extension-shear coupling (Ref. 41). In Ito and Chou's (Ref. 11) analytical model, the analysis is conducted in the *x-z* plane (see Appendix) rather than the *x-y* plane as in standard classical laminate theory. As such, $A_{16}$ and $A_{26}$ relate *x*- and *z*-direction extension to through-thickness (*xz*) shear. Furthermore, these components vary along the composite.

These components, normalized with their initial values at no shifting $A^0_{16}$ and $A^0_{26}$, are plotted along the laminate (from $x/\lambda = 0.5$ to $x/\lambda = 1$) for different values of shifting $\phi$ in Figure 6. In this figure, the color represents a curve obtained for a certain shifting value (as indicated by the colorbars). Clearly, when the layers are perfectly aligned on top of each other ($\phi = 0$), the magnitude of these components attain maximum value. In contrast, when the layers are completely shifted ($\phi = 0.5\lambda$) both of the components become completely suppressed. Thus, one observes that the drastic changes in the effective elastic properties when layer shifting increases (Figure 5(a)) can be attributed to the vanishing in-plane extension/out-of- plane shearing coupling effect shown in Figure 6.

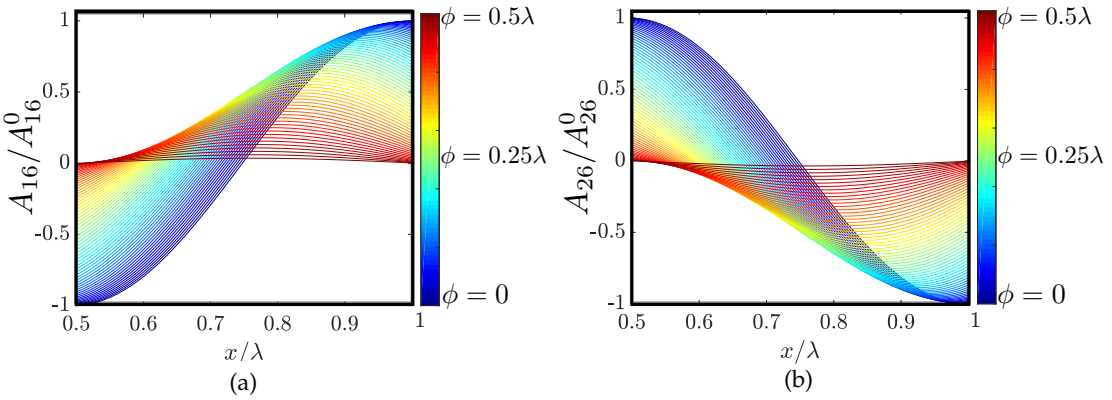


Figure 6.—Shear-extension coupling components of the classical laminate theory ***A*** matrix normalized with the initial value in the no shifting configuration ($^0$) along the laminate in the analytical model (Appendix) and their variation with layer shifting $\phi$. (a) $A_{16}$, (b) $A_{26}$.

The increase in $E_{xx}$ from no shifting to maximum shifting has also been reported experimentally by Ito and Chou (Ref. 11), albeit for a different carbon/epoxy material system. In order to compare the present numerical and analytical results to these authors' experimental results, the ratio of $E_{xx}$ at maximum shifting and perfectly aligned layers ( $E_{xx}^{\max}/E_{xx}^0$ ) is shown in Figure 5(c). The uncertainty from experimental data of (Ref. 11) was calculated using an error propagation theory for quotients (Ref. 42). The resemblance between the experimental results and the present numerical and analytical results, lends credence to the validity of the models presented herein. Furthermore, the fact that all three agree on the maximum effect of the layer shifting, suggests that layer shifting can be quite important in comparison to other mesostructural variabilities present in the experimental samples such as voids, local changes in volume fractions and fiber misalignments, to mention a few (Refs. 16, 17, and 43).

Regarding the drastic decrease in global Poisson's ratio, this has been also observed experimentally by (Ref. 26), who tested single layers and woven laminates of several layers. This effect might be partially due to the layer shifting effect. In contrast, the global out-of-plane shear modulus $G_{xz}$ show changes of no more than $\sim$ 5% and the changes in global $E_{zz}$ and $G_{xy}$ are practically negligible. However, to the knowledge of the authors, there is no experimental data available for comparison.

## 5.3 Influence of Layer Shifting on Damage Development

Since layer shifting affects the various elastic constants to very difference extents, it is expected that damage nucleation will be affected differently for every loading scenario as well. The effect of layer shifting in the global stress-strain responses due to damage evolution are presented here. These are obtained as follows. First, the degraded elastic properties are obtained from the homogenized damaged stiffness tensor ***C*** at a given strain level by using the boundary conditions described in the Section 4.1. Then, these properties are used to obtain the global stress-strain responses. This procedure is applied to the no shifting and maximum shifting configurations, since they should act as the lower and upper the bounds in the mechanical response.

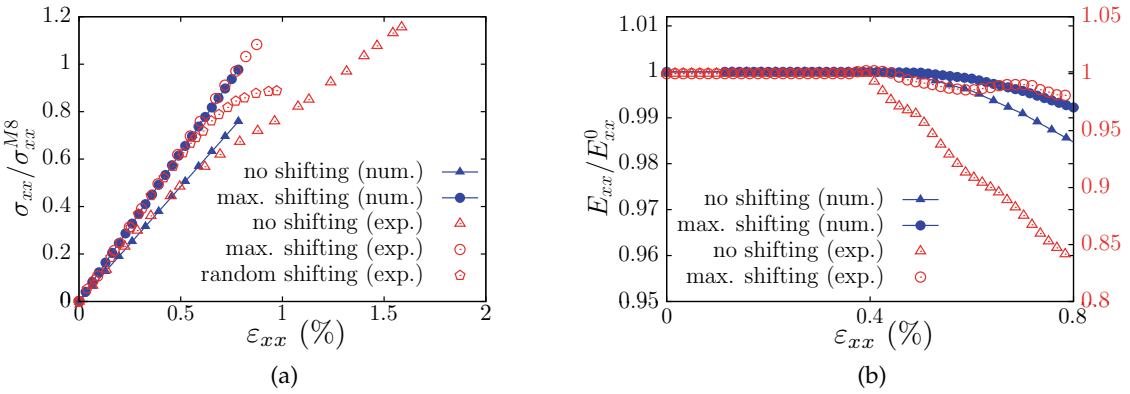


Figure 7.—Numerical (num.) and experimental (exp., (Ref. 11)) nonlinear behavior of the plain WCs under uniaxial extension. (a) Stress-strain curves, (b) global in-plane modulus degradation.

### 5.3.1 Global Uniaxial Extension Response

In Figure 7(a), stress-strain curves under uniaxial extension are compared to experimental results of Ito and Chou (Ref. 11), who also reported a random shifting configuration laying between the bounds given by perfectly aligned layers and maximum shifted layers. It must again be emphasized that the experiments represent a different carbon/epoxy composite than that modeled herein. However, valid qualitative comparisons can be made by properly normalizing the results. The stress values are normalized by their numerical and experimental values in the maximum shifting configuration at $\varepsilon_{xx} = 0.8\%$ ($\sigma_{xx}^{M8}$), where the simulations were stopped. The evolving value of $E_{xx}$ at different strain levels is normalized with the undamaged value $E_{xx}^{0}$, Figure 7(b). The damage development of the no shifting and maximum shifting configurations shows qualitative similarities with the experiments, although damage in the model is considerably more moderate. In both numerical models and experiments, the no shifting configuration tends to result in more damage, whereas in the maximum shifting configuration, the damage is limited. The maximum shifting model shows a curve that is more linear up to the failure when compared to the no shifting configuration (Figure 7(a)).

The contour plots of the damage variables in the fiber direction, Figure 8, can explain the different damage development in the maximum shifting and no shifting configurations. For the no shifting configuration, it can be observed that the largest amount of damage is developed within the pure matrix zones where the yarn undulation is minimum and the damage within the yarns is moderate. This correlates with the greater degree on nonlinearity for the no shifting case in Figure 7(a). In contrast, in the maximum shifting configuration, the damage is mainly developed in the yarns in the fiber direction. The pure matrix regions develop considerably less amount of damage when it is compared to the no shifting configuration. This correlates with less nonlinearity and the more brittle behavior for the maximum shifting case in Figure 8(a). These results suggest that layer shifting can have a significant impact on the character of damage growth and nucleation in woven composites. Clearly, the common practice of ignoring layer shifting when modeling woven composites could lead to prediction of erroneous damage mechanisms compared real, multilayered woven composites.

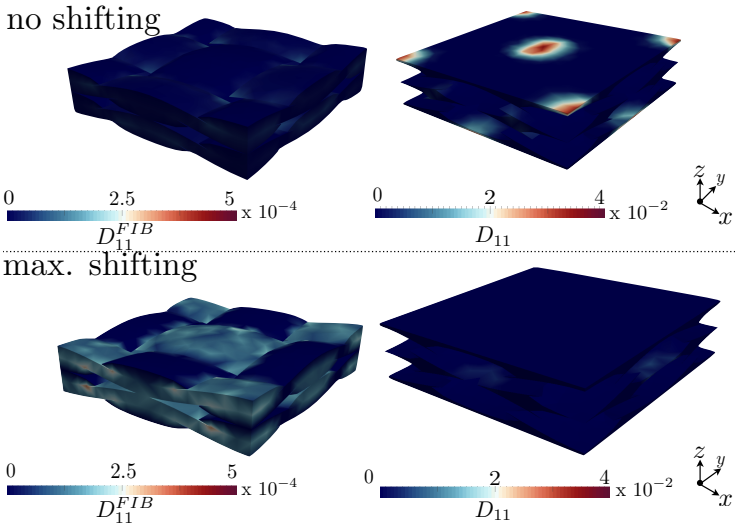


Figure 8.—Damage variables $D_{11}^{Fib}$ and $D_{11}$ in the yarns and matrix for the no shifting and maximum shifting configurations at $\varepsilon_{xx}$ = 0.8%.

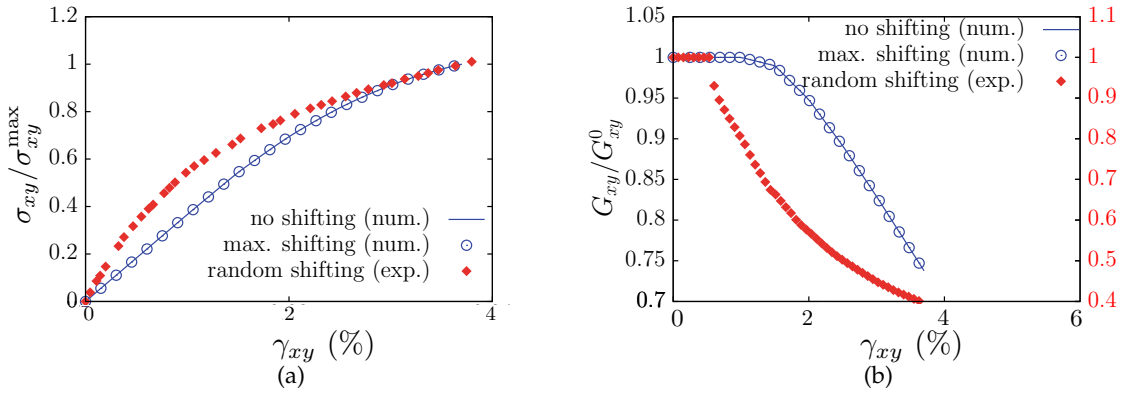


Figure 9.—Numerical (num.) and experimental (exp., (Ref. 44), Random shifting) nonlinear behavior of the plain WCs under in-plane shear extension. (a) Stress-strain curves, (b) global in-plane shear modulus degradation.

### 5.3.2 Global In-Plane Shear Response

In Figure 9(a), the stress-strain curves obtained in global in-plane shear are compared to experimental results (Ref. 44), where the shifting was uncontrolled, i.e., random. Once again, the carbon/epoxy material systems are not the same, but through normalization, valid qualitative comparisons can be made. The experimental response for this random configuration is compared to the numerical results for the no shifting and maximum shifting configurations, which should act as upper and lower bounds for the uniaxial loading case discussed before. The stress values of the curves are normalized with their stress levels at the maximum strain of $\gamma_{xy}$ = 3.7% achieved in the simulations.

In Figure 9(b), the global shear modulus degradation $G_{xy}$ (normalized with is initial value $G_{xy}^{0}$) is shown at different shear strains $\gamma_{xy}$. Here, larger strain levels are achieved in both numerical models and experiments compared to the uniaxial case discussed above. For both the no shifting and maximum shifting configurations, a high degree of nonlinearity is observed, which is also reflected in the

experiments. The global stress-stress curves for both the no shifting and maximum shifting configurations are similar and therefore it is predicted that damage development is not highly dependent on the layer shifting. This can be confirmed by observing the contour plots of the damage variable $D_{12}$ shown in Figure 10 where one can see that for both shifting configurations, damage is developed in the regions of yarns' undulation, and does not depend on the interaction between layers. Therefore, for the composite considered herein, it appears that damage under in-plane shear is yarn undulation-dominated mechanism and layer shifting has a negligible effect on damage development. This result also agree with the observations of (Ref. 7), where it was observed that nonlinearity in the global stress-strain curves under shear loading was due to damage within the composite yarns themselves, rather than from damage development in the matrix. The negligible effect of the layer shifting in the global in-plane shear response might be expected from the elastic response where negligible changes were observed for the in-plane shear modulus with respect to layer shifting (Figure 5(b)).

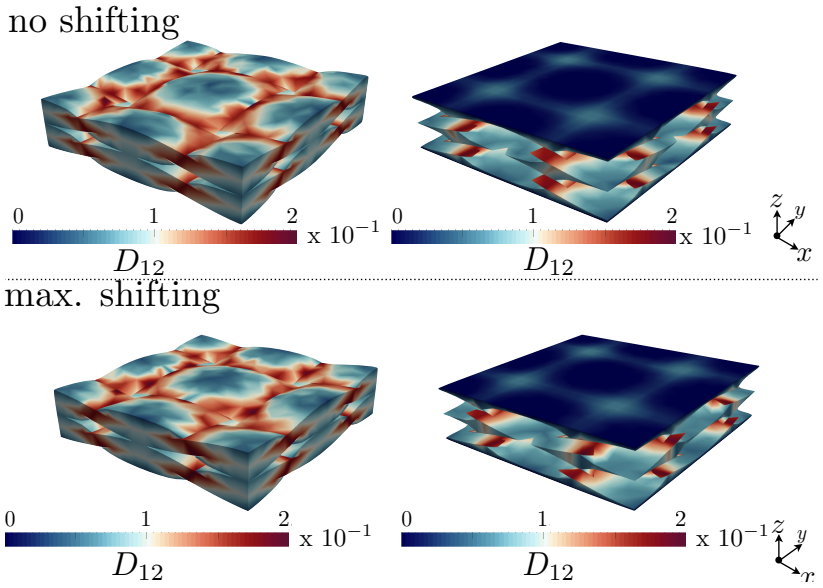


Figure 10.—Damage variables $D_{12}$ in the yarns and matrix for the no shifting and maximum shifting configurations at $\gamma_{xy}$ = 3.7%.

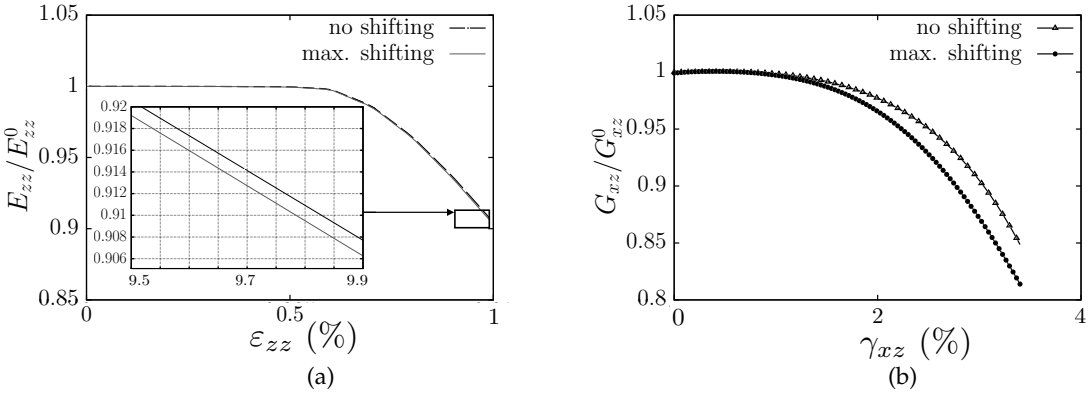


Figure 11.—Global out-of-plane properties degradation. (a) $E_{zz}$, (b) $G_{xz}$.

### 5.3.3 Global Out-of-Plane Response

The degradation of the global out-of-plane elastic modulus, $E_{zz}$, and shear modulus, $G_{xz}$, due to the corresponding out-of-plane $\varepsilon_{zz}$ and $\gamma_{xz}$ extensions, are presented in Figure 11(a) and (b). To the authors' knowledge there are no reported experiments for comparison. However, normal damage in the *z*-direction develops in similar fashion for both the no shifting and maximum shifting configurations, suggesting a negligible influence of layer shifting. This negligible effect was also observed in the $E_{zz}$ modulus of global elastic response (Figure 5(a)).

Regarding the out-of-plane shear modulus $G_{xz}$, the maximum shifting model shows more pronounced damage development than for the no shifting model at higher strain levels. This is also linked to the elastic response in the Figure 5(a), where a slightly increase of $G_{xz}$ with the layer shifting was observed. The higher levels of damage developed are thus a consequence of higher out-of-plane interactions in the transverse yarns when layers are shifted, and leading to more damage in the yarns.

As mentioned, a true quantitative comparison between the results of the present numerical model and the experimental results from the literature was not possible due to differences in the material systems. This difference includes not only the matrix and fiber materials, but also the overall and yarn fiber volume fractions. In a future investigation, the influence of the damage development at different volume fractions and shifting configurations will be carried out together with the development of detailed yarn micromechanics models for the accurate description of the damage development in a lower scale.

## 6.0 Conclusions

The effect of layer shifting on the global elastic and damage responses of woven composite laminates has been investigated with numerical models and compared to experiments and an analytical model from the literature. It has been found that most of the global elastic properties vary in a nonlinear fashion with layer shifting. The most pronounced effects were in the in-plane modulus of elasticity and Poisson's ratio, varying as much as by 30 and 80%, respectively.

The damage development in woven composites under uniaxial extension was also affected by layer shifting. For a laminate with no shifting, it was observed that most of the damage is developed in the pure matrix regions causing a characteristic nonlinear global response. In contrast, in a laminate with a maximum shifting, the amount of damage in the matrix is decreased, and damage mainly concentrates in the yarns, causing an abrupt, more brittle-like, response. For global in-plane shear loading, damage was observed mainly in the vicinity of the yarn undulations, and the layer shifting effect was negligible. Regarding the out-of-plane response, damage development in the global out-of-plane direction was observed to be insensitive to layer shifting. However, layer shifting promotes higher damage levels in the global out-of-plane shear response.

The numerical results were in good qualitative agreement with available experimental results from the literature. Through appropriate normalization, valid comparisons were made to elucidate the similar trends present in the model predictions and the experimental data, even though the carbon/epoxy material systems were not the same. The model results indicate that layer shifting can have a dramatic effect on the linear and nonlinear behavior of woven composites, as has been observed experimentally. When ignoring layer shifting, as is commonly done in woven composites modeling, models may not even predict correct damage mechanisms. Such lack of fidelity can negatively impact the model's capability not only to assess material performance, but also to perform model-based materials design.

# Appendix—Analytical Model

An analytical model following the approach of Ito and Chou (Ref. 11) has been used to show the relation between the shear-extension coupling terms and how they are affected by layer shifting, $\phi$.

## Geometrical Description

Consider two woven composite layers on top of each other as shown in Figure 12, each one with thickness $2h_y$. Henceforth, the lower and upper layers will be distinguished with the superscripts *A* and *B*, respectively. The center lines $z_0$ of the longitudinal yarns, can be approximated with the sinusoidal functions,

$$z_0^A = -\frac{h_y}{2}\sin\left(\frac{2\pi}{\lambda}x\right) \tag{18.a}$$

$$z_0^B = 2h_y - \frac{h_y}{2}\sin\left(\frac{2\pi}{\lambda}\left(x+\phi\right)\right) \tag{18.b}$$

where $\phi$ is to account for the layer shifting of the upper layer with respect to the lower one.

The fiber directions for each layer are simply obtained as,

$$\theta^{A,B} = \tan^{-1}\left(\frac{dz_0^{A,B}}{dx}\right) \tag{19}$$

Since the thickness of each yarn is $h_y/2$, the upper and lower functions $z_u$ and $z_l$ defining upper and lower bounds of the longitudinal yarns are obtained,

$$z_u^{A,B} = z_0^{A,B} + \frac{h_y}{2} \tag{20.a}$$

$$z_l^{A,B} = z_0^{A,B} + \frac{h_y}{2} \tag{20.b}$$

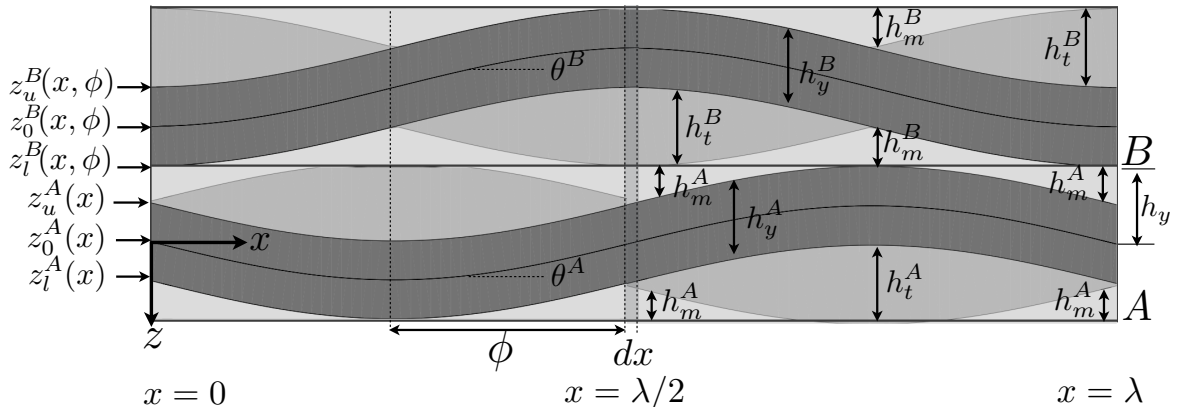


Figure 12.—Two-dimensional analytical simplification of the woven composite laminate.

The functions of transverse yarns $z_t$ ($h_t$ heights in Figure 12), that represent the domain of the yarns in the out of page ($y$)-direction, are obtained for the lamina $A$, and for the lamina $B$,

$$z_t^A(x)=\begin{cases}\dfrac{h_y}{2}\left(1+\sin\left(\dfrac{2\pi}{\lambda}x\right)\right) & x\le\lambda/2\\ \dfrac{h_y}{2}\left(\sin\left(\dfrac{2\pi}{\lambda}\left(\dfrac{\lambda}{2}-x\right)\right)-1\right) & x\ge\lambda/2\end{cases} \tag{21}$$

$$z_t^B(x)=\begin{cases}\dfrac{h_y}{2}\left(5+\sin\left(\dfrac{2\pi}{\lambda}(x+\phi)\right)\right) & x\in x\,|\,z_t^B\ge z_u^B\\ \dfrac{h_y}{2}\left(3-\sin\left(\dfrac{2\pi}{\lambda}\left(\phi-\dfrac{\lambda}{2}+x\right)\right)\right) & x\in x\,|\,z_t^B\le z_l^B\end{cases} \tag{22}$$

where $\lambda$ is the yarn wavelength.

## Laminate Properties

Considering the $x$-$z$ plane, Figure 12, the relations between the normal forces per unit length, $N$, and the strains, $\varepsilon$, generated in the $x$-$z$ directions are related by considering the extensional portion of classical laminate theory (Ref. 41) as,

$$\begin{bmatrix}N_x\\N_z\\N_{xz}\end{bmatrix}=\begin{bmatrix}A_{11}&A_{12}&A_{16}\\A_{12}&A_{22}&A_{26}\\A_{16}&A_{26}&A_{66}\end{bmatrix}\begin{bmatrix}\varepsilon_x\\\varepsilon_z\\\gamma_{xz}\end{bmatrix} \tag{23}$$

where the components of the matrix **A**, which vary with the $x$-coordinate $A_{ij}=A_{ij}(x)$, contain the contributions of each layer,

$$A_{ij}(x)=A_{ij}(x)^A+A_{ij}(x)^B \tag{24}$$

with,

$$A_{ij}^{A,B}(x)=h_y^{A,B}(x)\bar{Q}_{ij}^{A,B}(x)+h_t^{A,B}(x)Q_{ij}^t(x)+h_m^{A,B}(x)Q_{ij}^m(x) \tag{25}$$

where $h_y^{A,B}=z_u^{A,B}-z_l^{A,B}, h_t^{A,B}$ are the heights of the yarn's transverse sections and $h_m^{A,B}$ the heights of the matrix regions, as depicted in Figure 12. All these values are directly obtained with the previous expressions. $Q_{ij}$ are the reduced stiffness matrices for the laminates, yarns' transverse sections and matrix regions, represented with the superscripts $A$, $B$, $t$ and $m$, respectively. Observe that the line over $\bar{Q}_{ij}^{A,B}(x)$ means that rotation of the stiffness matrix in the fiber directions $\theta^{A,B}$ (Equation (19)) is taken into account following the typical notation used in classical laminate theory. The effective properties at an infinitesimal slice $dx$ (see Figure 12) are then calculated as functions of $x$ (Ref. 41),

$$E_{xx}(x) = \frac{dx}{a_{11}(x)H(x)} \tag{26.a}$$

$$E_{zz}(x) = \frac{dx}{a_{22}(x)H(x)} \tag{26.b}$$

$$G_{xz}(x) = \frac{dx}{a_{66}(x)H(x)} \tag{26.c}$$

where $a_{11}$, $a_{22}$ and $a_{66}$ are the components of the matrix $a(x) = \mathbf{A}^{-1}(x)$. The effective laminate properties are then taken as an average over the region $x(\lambda/2 \le x \le \lambda)$ as,

$$\bar{E}_{xx} = \frac{\lambda}{2}\int_{-\lambda/2}^{\lambda} E_{xx}(x)dx \tag{27.a}$$

$$\bar{E}_{zz} = \frac{\lambda}{2}\int_{-\lambda/2}^{\lambda} E_{zz}(x)dx \tag{27.b}$$

$$\bar{G}_{xz} = \frac{\lambda}{2}\int_{-\lambda/2}^{\lambda} G_{xz}(x)dx \tag{27.c}$$

## References


1. Rokbi M., Osmani H., Benseddiq N., Imad A. On experimental investigation of failure process of woven-fabric composites. Compos. Sci. Technol. 71 (2011) 1375–1384.
2. Bahei-El-Din Y., Rajendran A., Zikry M., A micromechanical model for damage progression in woven composite systems. Int. J. Solids Struct. 41 (2004) 2307–2330.
3. Lemaitre J.A. Course on Damage Mechanics. volume 1. Springer, Berlin, Heidelberg. 2 edition. 1996.
4. Barbero E.J., Lonetti P., Sikkil K.K. Finite element continuum damage modeling of plain weave reinforced composites. Composites Part B 37 (2005) 137–147.
5. Bednarcyk B.A., Stier B., Simon J.-W., Reese S., Pineda E.J., Meso- and micro-scale modeling of damage in plain weave composites. Composite Structures 121 (2015) 258–270.
6. Bednarcyk B.A., Stier B., Simon J.-W., Reese S. Investigation of micro-scale architectural effects on damage of composites. NASA Technical Report 2015-218740 (2015) 1–24.
7. Blackketter D.M., Walrath D.E., Hansen A.C. Modeling damage in a plain weave fabric-reinforced composite material. J. Compos. Tech. Res. 15 (1993) 136–142.
8. Zako M., Uetsuji Y., Kurashiki T. Finite element analysis of damaged woven fabric composite materials. Compos. Sci. Technol. 63 (2003) 507–516.
9. Matveev M., Long A., Jones I. Modelling of textile composites with fibre strength variability. Compos. Sci. Technol. 105 (2014) 44–50.
10. Hoffman O. The brittle strength of orthotropic materials. Journal of Composite Materials 1 (1967) 200–206.
11. Ito M, Chou T.-W. An analytical and experimental study of strength and failure behavior of plain weave composites. J. Compos. Mater. 32 (1998) 2–30.
12. Doitrand A., Fagiano C., Hild F., Chiaruttini V., Mavel A., Hirsekorn M. Mesoscale analysis of damage growth in woven composites. Composites Part A 96 (2017) 77–88.
13. Green S., Matveev M., Long A., Ivanov D., Hallett S. Mechanical modelling of 3d woven composites considering realistic unit cell geometry. Compos. Struct. 118 (2014) 284–293.
14. Gao X.-L, Li K, Mall S. A mechanics-of-materials model for predicting youngs modulus of damaged woven fabric composites involving three damage modes. Int. J. Solids Struct. 40 (2003) 981–999.
15. Daggumati S., Paepegem W.V., Degrieck J., Xu J., Lomov S., Verpoest I. Local damage in a 5-harness satin weave composite under static tension: Part II meso-fe modelling. Compos. Sci. Technol. 70 (2010) 1934–1941.
16. Sevenois R., Garoz D., Gilabert F., Spronk S., Fonteyn S., Heyndrickx M., Pyl L., Hemelrijck D.V., Degrieck J., Paepegem W.V. Avoiding interpenetrations and the importance of nesting in analytic geometry construction for representative unit cells of woven composite laminates. Composites Science and Technology 136 (2016) 119–132.
17. Bodaghi M., Vanaerschot A., Lomov S., Correia N. On the variability of mesoscale permeability of a 2/2 twill carbon fabric induced by variability of the internal geometry. Composites Part A: Applied Science and Manufacturing 101 (2017) 394–407.
18. Choi J., Tamma K.K. Woven fabric composites part I: Predictions of homogenized elastic properties and micromechanical damage analysis. Int. J. Numer. Meth. Eng. 50 (2001) 2285–2298.
19. Lomov S.V., Ivanov D.S., Verpoest I., Zako M., Kurashiki T., Nakai H., Hirosawa S. Mesofe modelling of textile composites: Road map, data flow and algorithms. Compos. Sci. Technol. 67 (2007) 1870–1891.

20. Doitrand A., Fagiano C., Chiaruttini V., Leroy F., Mavel A., Hirsekorn M. Experimental characterization and numerical modeling of damage at the mesoscopic scale of woven polymer matrix composites under quasi-static tensile loading. Compos. Sci. Technol. 119 (2015) 1–11.
21. Carvalho N.D., Pinho S., Robinson P., An experimental study of failure initiation and propagation in 2d woven composites under compression. Compos. Sci. Technol. 71 (2011) 1316–1325.
22. Huang H.S. Influence of phase shift on the responses of woven laminated composites. Compos. Struct. 130 (2015) 143–154.
23. Espadas-Escalante J.J., van Dijk N., Isaksson P. The effect of free-edges and layer shifting on intralaminar and interlaminar stresses in woven composites. Composite Structures 185 (2018) 212–220.
24. Doitrand A., Fagiano C., Leroy F.-H., Mavel A., Hirsekorn M. On the influence of fabric layer shifts on the strain distributions in a multi-layer woven composite. Compos. Struct. 145 (2016) 15–25.
25. Woo K., Suh Y.W., Whitcomb J.D. Phase shift effect on the stress distribution for satin weave composites. J. Compos. Mater. 36 (2002) 271–286.
26. Jekabsons N., Bystrom J. On the effect of stacked fabric layers on the stiffness of a woven composite. Composites Part B 33 (2002) 619–629.
27. Hansen N., Schreyer H. A thermodynamically consistent framework for theories of elastoplasticity coupled with damage. Int. J. Solids Struct. 31 (1994) 359–389.
28. Barbero E.J. Finite Element Analysis of Composite Materials Using ANSYS. Taylor and Francis book. CRC Pressr, Boca Raton, FL. 2014.
29. Weibull W.A. statistical distribution function of wide applicability. Journal of Applied Mechanics 18 (1951) 293–296.
30. T300 Carbon Fiber Technical Datasheet. TORAYCMA. 2017. Https://www.toraycma.com/, revised on March, 2018.
31. Paley M., Aboudi J. Micromechanical analysis of composites by the generalized cells model. Mech. Mater. 14 (1992) 127–139.
32. Bednarcyk B.A., Stier B., Simon J.W., Reese S., Pineda E.J., Arnold S.M. Damage Analysis of Composites Using a Three-Dimensional Damage Model: Micro-Scale Architectural Effects. Proceedings of the American Society for Composites 2014-Twenty-ninth Technical Conference on Composite Materials: Destech Publications Incorporated.
33. Aboudi J., Arnold S., Bednarcyk B. Micromechanics of Composite Materials: A Generalized Multiscale Analysis Approach. Butterworth-Heinemann. 2013.
34. Long A., Brown L. Modelling the geometry of textile reinforcements for composites: Texgen. in: Boisse P (Ed.), Composite Reinforcements for Optimum Performance. Woodhead Publishing Series in Composites Science and Engineering. Woodhead Publishing. 2011. pp. 239–264.
35. Doitrand A., Fagiano C., Irisarri F.-X, Hirsekorn M. Comparison between voxel and consistent meso-scale models of woven composites. Composites Part A: Applied Science and Manufacturing 73 (2015) 143–154.
36. Pietruszczak S., Mrz Z. Finite element analysis of deformation of strain-softening materials. Int. J. Numer. Meth. Eng. 17 (1981) 327–334.
37. Terada K., Horib M., Kyoyac T., Kikuchid N. Simulation of the multi-scale convergence in computational homogenization approaches. Int. J. Solids Struct. 37 (2000) 2285–2311.
38. Suquet P. Elements of homogenization for inelastic solid mechanics. in: Springer (Ed.), Homogenization techniques for composite media, Lecture Notes in physics 272. Sanchez-Palencia E., Zaoui A., editors. Wien. 1985. pp. 193–278.

39. Espadas-Escalante J.J., van Dijk N.P., Isaksson P. A study on the influence of boundary conditions in computational homogenization of periodic structures with application to woven composites. Compos. Struct. 160 (2017) 529–537.
40. Liu X., Rouf K., Peng B., Yu W. Two-step homogenization of textile composites using mechanics of structure genome. Compos. Struct. 171 (2017) 252–262.
41. Hyer M. Stress analysis of fiber-reinforced composite materials. volume 1 of 10. DEStech publications Inc., Lancaster, Pennsylvania. 2 edition. 2009.
42. Taylor J. Introduction to Error Analysis. A series of books in physics. University Science Books. 1997.
43. Zeman J., Sejnoha M. Homogenization of balanced plain weave composites with imperfect microstructure: Part I theoretical formulation. International Journal for Solids and Structures 22 (2004) 65496571.
44. Medina C., Canales C., Arango C., Flores P. The influence of carbon fabric weave on the in-plane shear mechanical performance of epoxy fiber-reinforced laminates. J. Compos. Mater. 48 (2014) 2871–2878.